Mixing versus Polymer Chemistry in the Synthesis of Loaded Polymer Nanoparticles through Nanoprecipitation

Antoine Combes, Corentin Rieb, Lucie Haye, Andrey S Klymchenko, Christophe Serra, Andreas Reisch

Mixing *versus* Polymer Chemistry in the Synthesis of Loaded Polymer Nanoparticles through Nanoprecipitation

Antoine Combes,[‡a] Corentin Rieb,[‡a] Lucie Haye,[a] Andrey S. Klymchenko,[a] Christophe Serra,[b] Andreas Reisch*[a, c]

a) Université de Strasbourg, CNRS, Laboratoire de Bioimagerie et Pathologies UMR 7021, Strasbourg F-67000, France; E-mail: reisch@unistra.fr.

b) Université de Strasbourg, CNRS, Institut Charles Sadron UPR 22, F-67000 Strasbourg, F-67000, France; E-mail: ca.serra@unistra.fr.

c) Université de Strasbourg, INSERM, Biomatériaux et Bioingénierie, UMR_S 1121, Strasbourg F-67000, France.

[‡] These authors contributed equally.

Keywords:

Nanoprecipitation, polymer nanoparticles, kinetics, microfluidics, mixing, polymer chemistry

Abstract

Polymer nanoparticles (NPs) loaded with drugs and/or contrast-agents have become key tools in the advancement of nanomedicine, requiring robust technologies for their synthesis. Nanoprecipitation is a particularly interesting technique for the assembly of loaded polymer NPs, which is well known to proceed under kinetic control, with a strong influence of assembly conditions. On the other hand, the nature of the used polymer also influences the outcome of nanoprecipitation. Here, we investigated systematically the relative effects of mixing of the organic and aqueous phases and polymer chemistry on the formation of polymer nanocarriers. For this, two mixing schemes, manual mixing and microfluidic mixing using an impact-jet micromixer, were first evaluated, showing, respectively, mixing times of several tens of milliseconds and a few milliseconds. Copolymers of ethyl methacrylate with charged and hydrophilic groups and different polyesters (PLGA, PLA) were combined with a fluorescent dye salt and tested for particle assembly using this “slow” and “fast” mixing. Our results showed that in case of the most hydrophobic polymers the speed of mixing had no significant influence on the size and loading of the formed NPs. In contrast, in the case of less hydrophobic polymers, faster mixing led to smaller sized NPs with better encapsulation. The switch between mixing and polymer controlled assembly was directly correlated to the solubility limit of the polymers in acetonitrile-water mixtures, with a critical point for solubility limits between 15 and 20 vol% water. Our results provide simple guidelines on how to evaluate the possible influence of polymer chemistry and mixing on formation of loaded NPs, opening the way to fine tuning their properties and optimizing their large scale production.

Introduction

Loaded polymer nanoparticles (NPs) are one of the corner-stones of nanomedicine.[1,2] The possibility to encapsulate various kinds of loads, ranging from drugs to contrast agents, and to direct and/or deliver these to nearly every part of the body, has allowed significant advances in diagnosis and therapy. Among the different techniques developed for the synthesis of such loaded polymer NPs, nanoprecipitation has proven to be a particular versatile and simple approach, which does not require high amounts of energy and can easily avoid the use of hazardous solvents or stabilizers.[3–6] In nanoprecipitation a solution of a polymer and the load in a water miscible organic solvent is mixed with an aqueous phase, inducing phase separation and the formation of NPs. A very interesting feature of nanoprecipitation is that the load is kinetically trapped inside the polymer matrix during synthesis, which allows using processing parameters rather than drug design to optimize the encapsulation of the load.

The kinetically controlled nature of nanoprecipitation has the consequence that the way and speed of mixing of the two phases can strongly influence particle formation and through this size, size distribution, and loading. In consequence, mixing parameters were strongly improved, from dropwise addition to the use of specifically designed mixers using collision of flows or herringbone mixers. [5,7–9] In these cases, it has been observed that improved mixing leads in general to smaller NPs with narrower size distributions.[3,10] Related to this are various parameters that indirectly influence the kinetics of particle formation. Among these are the concentration of polymer and load,[11,12] and the organic solvent used.[13,14] While the former influences the diffusion distances, the latter influences the limit of solubility of the polymer in the water-solvent mixture.

On the other hand, it was also observed that the nature of the polymer, notably its chemical composition and architecture, can influence the synthesis and the properties of NPs. For example, the relative and total length of the hydrophilic blocks in block copolymers could be used to control particle formation.[15] Furthermore, charged groups on the polymers have been shown to reduce particle size,[12,16–18] as was also the case with hydrophilic groups.[19]

In the present work, we thus wanted to evaluate the relative importance of polymer nature, i.e. different types of backbones and side groups, and mixing on the preparation of loaded polymer NPs. For this, we compared NPs prepared manually, corresponding to “slow mixing”, to NPs prepared using an impact-jet mixer, which has been shown previously to yield particularly small NPs, supposedly due to very efficient and “fast” mixing.[10,20] Various kinds of polymer chemistries and architectures were then used for the preparation of NPs by these two approaches(**Scheme 1**): In particular, we used methacrylate based copolymers with various amounts of hydrophobic (ethyl, EMA), charged (carboxylic acid, sulfonate) and hydrophilic (hydroxyethyl methacrylate, HEMA) side groups; as well as the polyesters poly(lactic acid) (PLA) and poly(D-L-lactide-co-glycolide) (PLGA), and a block copolymer

of PLGA with polyethylenglycol (PLGA-PEG). The results were compared, on the one hand, in terms of sizes and size distributions, which give an overall idea of the particle formation. And, on the other hand, in terms of the photophysical properties of NPs loaded with R18/F5-TPB, the salt of a rhodamine B derivative with a bulky hydrophobic counterion, which are sensitive to its organization inside the NPs, and give an idea of the encapsulation process.

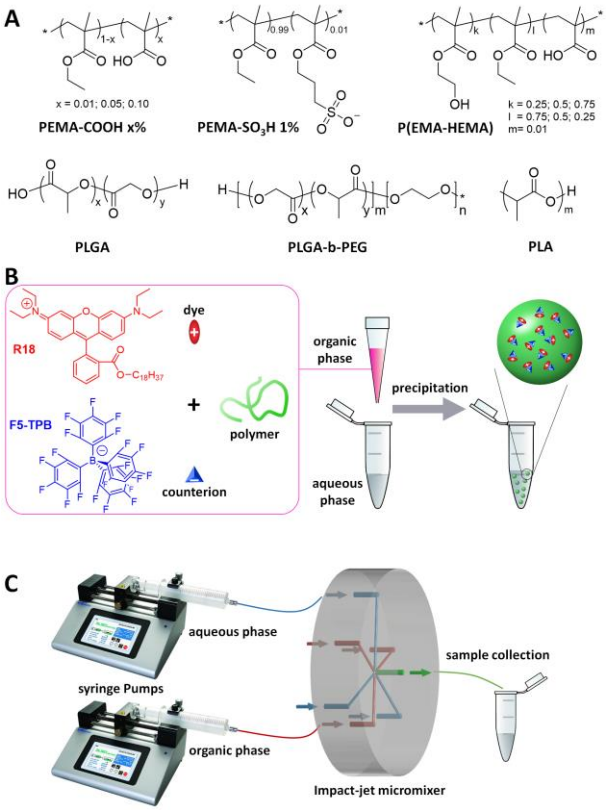

Scheme 1. (A) Structures of polymers used in this study (x y, k, l, m, n stand for mole fractions). (B) Structures of dyes and principle of manual nanoprecipitation. (C) Set-up for nanoprecipitation using the impact-jet micromixer.

Materials and Methods

Materials

The polymers poly(D-L-lactide-co-glycolide) (PLGA, acid terminated, lactide:glycolide=50:50, Mw 24,000-38,000 g.mol^{-1}, Ref.: 719870, Lot: BCBV0402), poly(lactic acid) (PLA, acid terminated, M_w 10,000-18,000, Ref : 719978, Lot : STBD0490V), poly(ethylene glycol) methyl ether-*block*-poly(L-lactide-co-glycolide) (PLGA-*b*-PEG, with PEG M_n 5,000 and PLGA M_w 25,000 lactide 50 mol%, glycolide 50 mol%, Ref : 799041, Lot: MKCL2095) were purchased from Sigma-Aldrich. For polymerization we used ethyl methacrylate (EMA, Sigma-Aldrich, >99%, Ref. 234893), methacrylic acid (MAA, Sigma-Aldrich, Ref. 155721), hydroxyethyl methacrylate (HEMA, Sigma-Aldrich, >99%, Ref. 477028), 3-sulfopropyl methacrylate potassium salt (Sigma-Aldrich, Ref. 251658), and azobisisobutyronitrile (AIBN, 98% from Fluka, recrystallized in ethanol). Monomers were typically purified over column.

Dimethylformamide (DMF, analytical grade), methanol (MeOH, analytical grade), and acetonitrile (analytical reagent ≥99.5%) were obtained from Carlo-Erba. Potassium iodate (Sigma Aldrich, 99.5% Ref. 215929, Lot: MKCP8518), potassium iodide (AlfaAesar, 99%, Ref. A12704, Lot: 10194063), boric acid (ThermoFisher, 99.8%, Ref. 012680.A1, Lot: P16H103), sodium hydroxide (10 M solution, FisherScientific, Ref. J/7620C/05, Lot: 2177558), sulfuric acid (5 M solution, FisherScientific) were used as received. R18/F5-TPB was synthesized from rhodamine B octadecyl ester perchlorate (Sigma-Aldrich, >98.0%) and lithium tetrakis(pentafluorophenyl)borate ethyl etherate (AlfaAesar, 97%) through ion exchange followed by purification through column chromatography as described previously.[21,22] Phosphate buffer (20 mM, pH 7.4) was prepared from Na_2HPO_4, ≥99% and NaH_2PO_4 H_2O, ≥98% (both Sigma-Aldrich). MilliQ water was used in all experiments.

Polymer Synthesis

Ehtyl methacrylate (EMA) based copolymers with different charged or hydrophilic comonomers were synthesized through free radical polymerization. Monomers were dissolved in DMSO and mixed at the desired ratio in a round bottom flask. 0.01 eq. of AIBN was added, the mixture was flushed with argon for 5 min and heated at 70 °C under inert atmosphere. The advancement of the reaction was monitored using NMR spectroscopy. Once the conversion had reached 25%, the polymerization was stopped by quickly lowering the temperature. Conversion was kept to relatively low values to avoid strong variations in copolymer composition. The mixture was precipitated in methanol or water/methanol mixtures if necessary, redissolved in acetonitrile and precipitated a second time before drying and characterization. NMR spectra were recorded at 20 °C on a BrukerAvance III 400 spectrometer and were used to evaluate polymerization conversion and characterize the final polymers.

As an example, the synthesis of PEMA-COOH-5% is given, further details can be found in the ESI:

Monomers were dissolved in DMSO at a concentration of 2 M. 50.8 mL of EMA (102 mmol, 95 eq.) and 2.67 mL of MAA (5.35 mmol, 5 eq.) solutions were placed in a 100 mL round-bottom flask. 4.49 mL of AIBN at 40 mg/mL (1.10 mmol, 1 eq.) were added and the mixture was flushed with argon during 5 min. It was then heated at 70 °C under inert atmosphere for 30 min and an aliquot was taken and analyzed using ^{1}H NMR spectroscopy. The ratio between the intensities of the O-CH_2- signals from the monomer and the polymer showed 31% of conversion. The mixture was precipitated in 400 mL of a methanol-water 9/1 mixture. The polymer was collected after centrifugation and redissolved in acetonitrile before a second precipitation in methanol at 0°C. The obtained polymer was dried under vacuum to give 2.60 g of white solid (overall yield 22 %). ^{1}H NMR (400 MHz, $CDCl_3$) δ (ppm): 4.03 (m, 2H), 2.09 – 1.73 (m, 2H), 1.37 – 1.18 (m, 3H), 1.13 – 0.78 (m, 3H).

Methods

Preparation of NPs: Stock solutions of polymers were prepared at a concentration of 10 $g.L^{-1}$ in acetonitrile, containing 30 vol% methanol, where needed. These solutions were diluted to 2 $g.L^{-1}$ in acetonitrile containing 5 wt% or 30 wt% of R18/F5-TPB (relative to the polymer, for polyesters and polymethacrylates, respectively). For manual preparation, this solution was quickly added to a 9-fold volume excess of MilliQ water or phosphate buffer (20 mM, pH 7.4) under shaking (Thermomixer comfort, Eppendorf, 1100 rpm at 21°C). For preparation using microfluidics, we used an impact-jet (KM) mixer, whose structure consists of three steel plates, namely the inlet, mixing and outlet plates.[23] Both inlet fluid streams are split into 3 sub-streams thanks to microchannels of 120 µm. Then the alternated 6 sub-streams converge to a single pine hole of 300 µm, where they are mixed by frontal collision. In this case, the organic solution was mixed in a ratio 1:9 with MilliQ water or phosphate buffer (20 mM, pH 7.4), based on the flow rates, at global volume flow rates of 2, 5, or 10 $mL.min^{-1}$, using two KDS Legato™ 100 Infuse Only Syringe Pumps from KD Scientific. Considering the geometry of the mixer, these volume flow rates correspond to flow speeds of 0.77, 1.93 and 3.86 $m.s^{-1}$. Samples were taken after about 30 s of stabilization at the given flow rates. The particle solutions were analyzed directly after suitable dilution, without purification in order to better visualize the effects of preparation conditions.

Dynamic light scattering (DLS): A Zetasizer Nano series ZSP (Malvern Instruments S.A.) was used for size measurements at 25 °C. Each of the samples was measured 10 times with a run length of 10 s each. The measurement position was fixed to 4.3 mm and the attenuation was adjusted automatically. The volume average values were used, which are determined by the Zetasizer software (Malvern) based on Mie theory. For density, viscosity, and refractive index, we used the values integrated in the Zetasizer software for water. The actual values in mixtures containing 10 vol% of acetonitrile (the maximum), can deviate by, respectively, 2%, 10%, and 1% for density, viscosity, and refractive index,[24,25] which might lead to a slight error in the absolute values, but does not affect comparison between different formulations and types of preparation. Mean values represent the average over at least three independent preparations, error bars correspond to the standard deviation over the means from different preparations.

Transmission electron microscopy (TEM): Solutions of NPs (10 µL) were deposited onto carbon-coated copper−rhodium electron microscopy grids following amylamine glow-discharge. They were then treated twice for 10 s with a 2% uranyl acetate solution for staining. The obtained grids were observed using a Tecnai F20 Twin transmission electron microscope (FEI Eindhoven Holland) operating at a voltage of 200 kV. Images (1,024 pixels × 1,024 pixels) were recorded using a US1000 camera (Gatan) and analyzed using the Fiji software. At least 200 particles per condition were analyzed.

Absorption and emission spectra: Absorbance spectra were measured with a Cary 5000 Scan ultraviolet−visible spectrophotometer (Varian) between 400 and 800 nm. Fluorescence spectra were measured using an Edinburgh FS5 spectrofluorometer equipped with a thermostated cell compartment between 570 and 800 nm with wavelength of excitation equal to 535 nm. Alternatively, a Tecan Plate Reader was used for quantum yield (QY) measurements. The measurements were performed in tissue culture test plates 96f with 100 µL of sample in each well. Excitation was performed at 535 nm. Emission spectra of the dye-loaded NPs in aqueous solution and of Rhodamine 101 in ethanol as reference were recorded. QYs were calculated using a relative method:

$$QY_{NP} = QY_{R101}\frac{F_{NP}/A_{NP,530nm}n_{H_2O}^2}{F_{r101}/A_{r101,530nm}n_{EtOH}^2} \quad (1)$$

where F_{NP} and F_{R101} represent the emission intensity integrated over the entire emission wavelength range of the NP and rhodamine 101 solutions, respectively. $A_{NP,\ 535\ nm}$ represents their absorbance at the excitation wavelength. QY_{R101} is the QY of rhodamine 101, which was taken to be 95%[26], and n corresponds to the respective refractive indices of the solvents (1.33 for water and 1.36 for ethanol).

Turbidimetry: Turbidimetry measurements were performed on a Cary 5000 Scan ultraviolet−visible spectrophotometer (Varian) at 400 nm. For this, a solution of the polymer in ACN was titrated with MilliQ water. Polymer precipitation is detected by a drop in transmittance at 400 nm. Basically, we measured the transmittance of polymer solutions (2 $g.L^{-1}$) in acetonitrile. After addition of few µL of aqueous phase and homogenization, we remeasured the transmittance. We repeated the process at least until the transmittance decreased below 80%. The limit of solubility was taken to be the composition of the solution before the transmittance decreased below 80%. Experiments were performed at least in triplicate and the average values are given with the corresponding standard deviation or step size of the titration as error.

Determination of Micromixing Times:

Mixing times were determined following a procedure established by J-M. Commenge et al.[27]

Briefly, an acidic and a basic solution are mixed with a small excess of basic solution. The basic solution contains potassium iodide and iodate. The latter reacts with acid to form I_2, which then reacts with iodide to form I_3^-. This reaction only happens in case of inhomogeneous mixing, as it is in competition with the acid-base reaction (neutralization) that is much faster. The amount of I_3^- is measured by absorbance (OD) and is correlated to the speed of micromixing (higher I_3^- concentration corresponds to slower mixing).

Practically, stock solutions of potassium iodate (0.06 mol.L^{-1}), potassium iodide (0.32 mol.L^{-1}), boric acid (0.665 mol.L^{-1}), sodium hydroxide (1 mol.L^{-1}) and sulfuric acid (0.5 mol.L^{-1}) were prepared in degassed water.

Solutions of sulfuric acid were made at 0.04 mol.L^{-1} and 0.06 mol.L^{-1} (respectively for low and high speed of mixing). The basic solution was prepared by adding successively solutions of boric acid, sodium hydroxide, potassium iodide and potassium iodate to obtain a final concentration of 0.09 mol.L^{-1} of NaH_2BO_4, 0.032 mol.L^{-1} of potassium iodide and 0.006 mol.L^{-1} of potassium iodate. Both solutions were degassed by Argon bubbling for at least 10 minutes. Mixing of the two solutions was performed manually and using microfluidic mixing (2, 5 and 10 mL.min^{-1}).

After mixing, the absorbance was measured at 353 nm. From this, and taking into account the used concentrations, the segregation index X_S was calculated following procedures from the literature[27]:

$$X_S = \frac{Y}{Y_{segregated}} = \frac{\frac{2([I_2]+[I_3^-])}{[H^+]_0}}{\frac{6[IO_3^-]_0}{6[IO_3^-]_0+[H_2O_3^-]_0}} \qquad (2)$$

Using described models, the absorbance can be further used to estimate mixing times with the following equation: $t_m = 0.33(OD)[H^+]^{-4.55}[KI]^{-1.5}[KIO_3]^{5.8}[NaOH]^{-2}[H_3BO_3]^{-2}$. Experiments were performed in triplicate.

CFD modeling of flows: The Ansys Fluent software was used to model the flow at various flow rates, corresponding to the flow speeds calculated based on the mixer geometry. A geometry based on 6 converging entry channels of 120 µm x 120 µm width and a cylindrical outlet channel of 280 µm diameter and a length of 5 or 10 mm was used (**Figure 1** and **ESI Figure S1**). For the latter a mesh comprising 102 000 knots and 310 000 elements was used. A species model of acetonitrile and water was used to simulate the mixing assuming a mutual diffusion coefficient of 1.0 10^{-9} m^2.s^{-1}.[28] The ratio of volume flow-rates of the organic to aqueous phase was set to 1:9 based on the used entry velocities. Three different entry velocities were used for simulation corresponding to global volume flow rates of 2, 5, and 10 mL.min^{-1}. At least 100 iterations were applied for each condition. The results of the simulations were analyzed using the Ansys Fluent software. Graphical representation of flow speeds and mass fractions in the symmetry plane as well as in cross-sections situated 5 and 10 mm downstream from the point of injection were created. The uniformity indices of the distribution of the mass fractions of acetonitrile and water in the different cross-sections were established using functions built-in in Ansys Fluent.

Results and Discussion

Mixing

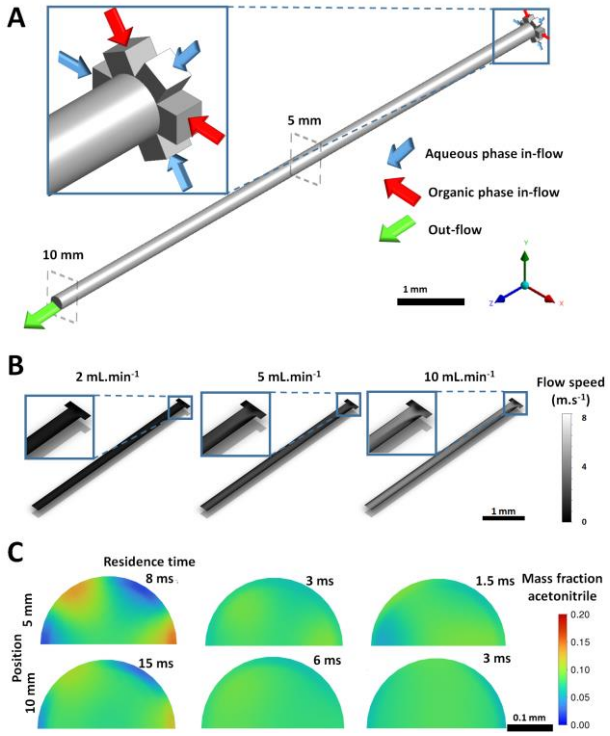

Figure 1. Simulation of fluid mixing between water and acetonitrile at different flow speeds using CFD: A) General geometry used for modelling, with indication of the considered in- and outflows and the cross-sections analyzed. The simulation was carried out on half the geometry, using the symmetry plane situated in the center of the channel. B) Velocity profiles along the symmetry plane for three global volume flow rates with an acetonitrile:water volume ratio of 1:9 (represented here for the first 5 mm). C) Mass fraction profiles of acetonitrile for cross-sections situated at 5 (top) and 10 (bottom) mm downstream, as indicated in (A). The residence time values indicate the mean residence time of the fluid up to the given position in the mixer. An identical color scale was used for all cross-sections going from 0 (blue) to 20 mass% acetonitrile.

In a first step, we aimed at quantifying as far as possible the mixing of the two fluid phases in the two approaches we used for nanoprecipitation, namely, manual mixing and microfluidic mixing by an impact-jet mixer. In manual mixing, the organic solution is added to a 9-fold excess of aqueous phase using a micropipette under shaking. In the impact-jet micromixer organic and aqueous phase are injected at a volume flow rate of 1:9 using syringe-pumps. Each inlet stream is divided into 3 sub-streams in 120 µm wide microchannels, followed by the convergence of the 6 sub-streams to a single, 300 µm wide pin-hole. We selected two very different approaches to quantify mixing speeds in these systems: Modeling using computational flow dynamics (CFD)[14,29] and indirect measurements using competitive reactions.

CFD was first used to simulate the flow in the impact-jet micromixer and through this to quantify the achieved mixing and its dependence on flow speed. In our case, we modeled the mixing of acetonitrile

and water in the impact-jet micromixer using the ANSYS Fluent software for the three volume flow rates. The considered geometry and obtained results are summarized in **Figure 1** and **Table 1** (as well as in the ESI **Figures S1** and **S2**) and show that, as expected, increasing the flow speed leads to improved mixing, in particular when going from a global volume flow rate of 2 mL.min^{-1} to 5 mL.min^{-1}. In order to obtain a quantitative idea of the mixing time, we analyzed the so-called uniformity index (1 for highest uniformity), used to quantify the extent of mixing, and related it to the residence time in the mixer for the different flow rates: In the case of 5 mL.min^{-1} very good mixing (uniformity index 0.96) is achieved after a residence time of 3 ms (Table 1). At 10 mL.min^{-1} a similar level of mixing (uniformity index 0.95) is achieved after only 1.4 ms. In the case of 2 mL.min^{-1}, it requires > 15 ms to reach corresponding mixing values. These results suggest that, according to CFD, mixing times at 10, 5, and 2 mL.min^{-1}, are of the order of 1 ms, 3 ms, and several tens of ms, respectively.

Table 1. Data on the quality of mixing depending on way of mixing and used flow rates, evaluated using competitive reactions and CFD simulation.

Mixing type	Flow rate	Mixing time[1)]	at 5 mm down-stream[2)]	
	(mL min^{-1})	(ms)	Residence time (ms)	Uniformity index
Manual	-	27 ± 5		
Impact-jet	2	28 ± 4	8	0.87
	5	2 ± 1	3	0.96
	10	<1	1.4	0.95

1) as obtained from the Villermaux-Dushman reaction
2) as obtained from CFD simulation

A second way to achieve a comparison of the different mixing conditions is the use of competitive reactions, which allows relating the ratio of the obtained products to the speed of mixing.[27,30,31] Here, we chose the Villermaux-Dushman reaction, in which neutralization of borate competes with the acid catalyzed redox reaction of iodate with iodide. Our choice was motivated by the simple quantification of product ratios through absorbance measurements and the fact that this reaction has been previously used to characterize similar mixers.[23,27,32] Again, the obtained segregation indices X_S (X_S = 0 for perfect micromixing, X_S = 1 for infinitely slow mixing) for the impact-jet mixer showed that increasing the flow rate effectively led to better, that is, faster mixing (**Figure 2**). The speed of manual mixing was of the same order of magnitude as mixing at the lowest flow rate used here (2 mL.min^{-1}). However, at high flow-rates (5 and 10 mL.min^{-1}) mixing in the impact-jet mixer led to clearly improved mixing, as indicated by the lower X_S values. These results were then used to estimate quantitatively the micromixing times based on a model proposed for this reaction:[27] For manual and slow microfluidic mixing, micromixing times of tens of ms were obtained (27 ± 5 ms and 28 ± 3 ms, respectively, **Table 1**). For faster flow, the obtained micromixing times were of the order of a few ms (2 ± 1 ms for 5

mL.min^{-1}) or even below 1 ms (for 10 mL.min^{-1}). Thus, the measured values were in good quantitative agreement with the simulated ones (considering a uniformity index of 0.9 – 0.95, **Table 1**). Furthermore, the measured values are comparable to previous evaluations, which found very fast mixing under these conditions.[23,32] Measurements in other types of impinging jet or multi-inlet-vortex mixers also yielded mixing times in the low ms range,[31,33] which is consistent with the results obtained here.

The combined results of CFD modeling and experimental measurement of micromixing using competitive reactions suggest that the microfluidic and manual approaches used here provide mixing of the aqueous and organic phases on two different time scales: very fast mixing in the case of the impact-jet mixer with mixing times on the low (<1 – 3) ms timescale and significantly slower mixing for manual mixing using a pipette and a shaker or low flow rates, for which mixing was at least one order of magnitude slower, resulting in mixing times of the order of tens of ms.

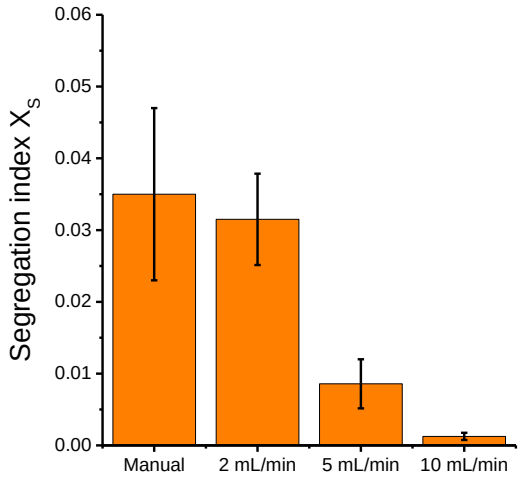

Figure 2. Segregation indices X_S (X_S = 0 for perfect micromixing, X_S = 1 for infinitely slow mixing) as obtained using the Villermaux-Dushman reaction for various mixing conditions either manually or using the impact-jet mixer. Experiments were performed in triplicate and error bars give the standard deviation.

Solubility of Polymers

The driving force of particle formation in nanoprecipitation is the insolubility of the polymer and the load in the final mixture obtained after mixing the organic and the aqueous phase. In a second step, we therefore determined the limit of solubility of the different polymers. For this, we used turbidimetry experiments, in which small quantities of MilliQ-water were added to solutions of the polymers at 2 g.L^{-1} in organic solution (acetonitrile or acetonitrile with 10 vol% methanol for the least hydrophobic), while measuring the transmittance. We considered that the solubility limit was reached when the measured transmittance at 400 nm dropped below 80%. In the case of the EMA polymers

with different percentages of charges (1 to 10%), the solubility limit was reached between 6 and 14 vol% water, as expected for copolymers with a high amount of hydrophobic monomers (Figure 3A). Increasing the amount of methacrylic acid groups only slightly shifted the solubility limit to higher water fractions. Sulfonate groups were more effective in increasing the solubility of the polymer, probably due to the fact that they are entirely in their deprotonated (salt) form in MilliQ water.

Increasing the fraction of hydrophilic HEMA monomers in statistical (random) EMA/HEMA copolymers led to a continuous (and practically linear) increase in the solubility limit, up to a water fraction of over 50 vol% for the copolymer bearing 75 mol% of HEMA monomers, in good agreement with previous observations.[19] Measurements on different polyesters showed that these had a somewhat higher solubility, with solubility limits in the range 12 to 20 %water, than the hydrophobic methacrylates, in particular PLA. The obtained values for the limit of solubility were in good agreement with results obtained previously by us[21] and others.[13] Interestingly, PLGA and the PLGA-PEG block copolymer had very similar solubility limits, practically independent of the presence of the PEG block. Performing the same type of experiments with the dye salt R18/F5-TPB alone using DLS yielded a solubility limit of about 6 vol% of water.

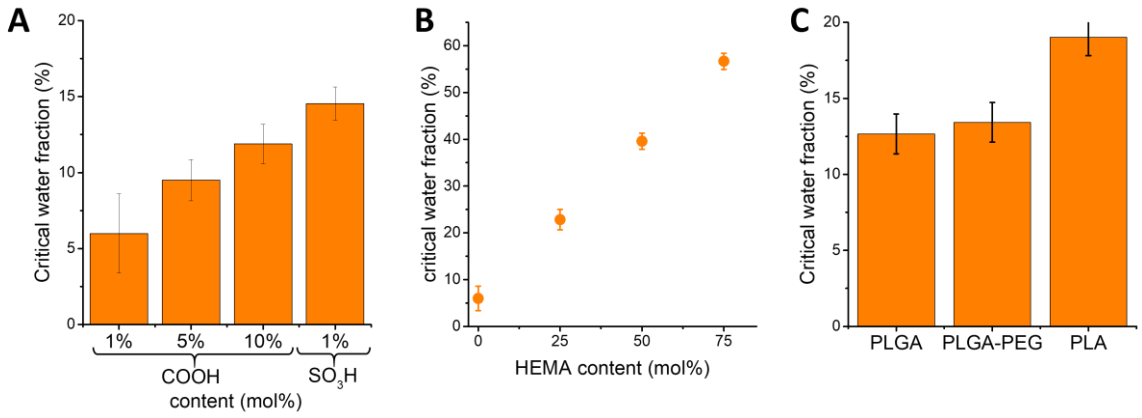

Figure 3. Limits of solubility of the different polymers as obtained from turbidimetry measurements by adding MilliQ water to a 2 g L^{-1} solution of the polymers in acetonitrile (containing up to 10% of methanol). A) PEMA with different fractions of COOH and SO_3H groups. B) P(EMA-HEMA) copolymers with different EMA/HEMA ratios. C) Different polyesters. Given is the highest fraction of aqueous phase in the mixture before the transmittance decreased below 80%. Mean values are triplicates of three independent measurements, error bars give the standard error of the mean.

Nanoparticles from Methacrylate Polymers

To evaluate the relative influence of polymer chemistry and speed of mixing on synthesis of NPs through nanoprecipitation, we started from methacrylate polymers having different types and amounts of side groups and architectures. In all cases 30 wt% (relative to the polymer) of the hydrophobic dye salt R18/F5-TPB were added to the organic phase. Microfluidic mixing using an

impact-jet micromixer was used as “fast” mixing and manual addition using a micropipette as “slow” mixing. On the one hand, particle size and size distribution were studied to gain a general insight into particle formation. On the other hand, absorbance and fluorescence measurements were used to study encapsulation of the load.

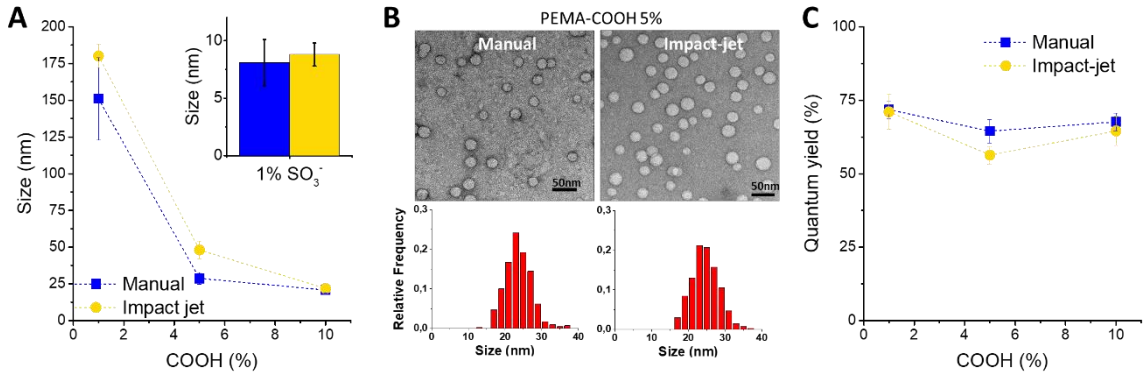

Figure 4. Sizes from DLS (A), TEM micrographs and histograms (B), and quantum yield (C) of NPs made from PEMA-COOH with different COOH fractions either manually or using an impact-jet mixer. NPs contained 30 wt% dye (R18/F5TPB). Nanoprecipitation was performed in phosphate buffer. The used flow rates were 5 mL.min^{-1} except for PEMA-COOH 1%, where 2 mL.min^{-1} was used in order to avoid aggregate formation. For DLS and QY mean values from three independent preparations are given. Error bars correspond to standard error of the mean. For TEM histograms at least 200 particles were analyzed per condition.

First, we applied this protocol to PEMA polymers bearing 1, 5, or 10 mol% of COOH groups (**Figure 4**). As observed previously, the particle size decreased strongly with increasing amount of (potentially) charged groups, going from >150 nm to <30 nm for 10 mol% COOH.[34] However, for these polymers fast mixing in the impact-jet mixer did not lead to the formation of smaller NPs than manual mixing (**Figure 4A**). A closer look on the particle sizes using TEM revealed no significant differences in the particle size distributions between particles made through fast or slower mixing (**Figure 4B**). A particular case was PEMA-COOH 1%, as preparation of particles at the highest flow rates led to the formation of aggregates, we decreased the flow rates accordingly to avoid this. The ζ-potential was clearly negative for both ways of mixing, e.g. for PEMA-COOH 5% - 21 mV for manual and -27 mV for preparation with the impact-jet micromixer (**ESI Table S1**). Using PEMA polymers bearing 1% of sulfonate groups (instead of COOH groups) gave NPs with very small sizes below 10 nm (**Figure 4A**), as observed previously.[18] Again no significant influence of the way of mixing was observed.

We further characterized these NPs using absorbance and fluorescence spectroscopy. Absorbance spectra (**ESI Figure S3A**) corresponded well to the expected absorbance of the used rhodamine dye and did not show major differences between those prepared manually and those prepared using fast microfluidic mixing, both in terms of intensity and shape. Indeed, the obtained absorbance values were in good agreement with those expected based on the concentration and the extinction coefficient of

the dye (measured 0.13, expected 0.15 for ε = 106 000 M^{-1} cm^{-1} in methanol). It should be noted that non-encapsulated R18/F5TPB dye salt has a strong tendency to aggregate, typically visible in the form of pink deposits at the sides or at the top of the tubes and leading to a corresponding decrease of the measured absorbance in solution.[22,35] Together with previous studies on encapsulation of this dye salt, which estimated the encapsulation efficiency to be > 95% using ultracentrifugation, dialysis, and observations on cell culture,[12,21,35] these results suggest a good encapsulation of the dye salt within the NPs.[35] Furthermore, they confirmed the correct performance of our impact-jet micromixer based system to yield the expected mixing ratios of the components.

Fluorescence emission spectra were also in excellent agreement in terms of their shape (**ESI Figure S3B**). The obtained spectra could then be used to determine the fluorescence quantum yield (QY) of the NPs (**Figure 4C**), which is directly related to the aggregation state of the dyes inside the NPs. Indeed, aggregation of dyes is known to lead to a decrease in the QY, often also seen from a relative increase in the absorbance at the shoulder (530 nm).[21] Here, QY measurements of the corresponding dye-loaded NPs showed very similar values in the range of 60 to 75% for NPs made from PEMA polymers bearing different amounts of COOH groups. In some cases, a slightly lower QY value for the NPs made using the impact-jet micromixer was obtained. However, the speed of mixing did, in general, not have a significant influence on the QY. For PEMA-SO_3H 1%, we did not observe a significant influence of the way of mixing on the QYs either, though these were with 58% somewhat lower than for the PEMA-COOH polymers (**ESI Figure S7**). Together with the absorbance results, this indicates that the speed of mixing does not have a significant influence on encapsulation of the dye salt for this series of polymers.

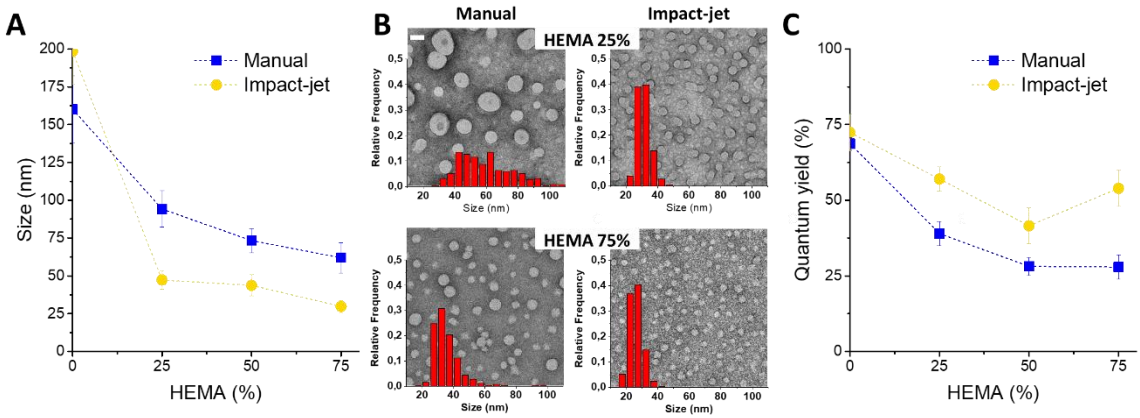

Figure 5. Sizes from DLS (A), TEM micrographs and histograms (B), and quantum yield (C) of NPs made from EMA-HEMA copolymers with different HEMA fractions either manually or using an impact-jet mixer. NPs contained 30 wt% dye (R18/F5TPB). Nanoprecipitation was performed in MilliQ water. The used flow rates were 10 mL.min^{-1} except for EMA 100%, where 2 mL.min^{-1} was used in order to avoid aggregate formation. For DLS and QY mean values from three independent preparations are given. Error bars correspond to standard error of the mean. For TEM histograms at least 200 particles were analyzed per condition.

Second, we varied the overall hydrophobicity of the polymer by using copolymers of EMA and HEMA with varying fractions of the two monomers. As expected from previous results,[19] we observed a decrease in particle size, as well as a decrease in QY with increasing fraction of hydrophilic groups in the polymer (**Figure 5A**). For HEMA contents starting from 25%, NPs prepared through fast mixing using the impact-jet micromixer showed significantly lower sizes in DLS than those prepared manually, e.g. for EMA/HEMA 25/75 decreasing form 62 nm for slow to 29 nm for fast mixing. TEM images confirmed a significant shift of the particle size distribution to smaller sizes for fast compared to "slow" mixing. Indeed, both the mean values (and modes) of the particle sizes and the sizes of the largest particles were significantly lower for the former. The ζ-potential was again clearly negative in both cases (e.g. -30 mV and -21 mV for EMA/HEMA 25/75, respectively, for manual and impact-jet mixing, **ESI Table S1**). At the same time, we observed significantly higher QYs for the dye-loaded NPs prepared through microfluidics, starting from 25% of HEMA content, e.g. from 28% for slow to 54% for fast mixing for EMA/HEMA 25/75. Thus, mixing has a distinctive influence on particle formation in the case of these polymers.

To understand further the influence of the mixing speed, we studied formation of NPs for two representative polymers, PEMA-COOH 5% and P(EMA-HEMA) 50/50 at various mixing speeds (ESI **Figure S4**, here with 5 wt% dye salt loading). In case of PEMA-COOH 5% a slight increase in size of the formed NPs was observed when going from slow to fast mixing, however, the size quickly reached a plateau. This indicated that the influence of the mixing speed is effectively weak. For P(EMA-HEMA) 50/50, a continuous decrease of particle size was observed for increasing flow and hence mixing speed up to at least 15 ml.min^{-1}.

Nanoparticles from Polyesters

In the next step, we extended our study to biodegradable polyesters frequently used in the assembly of NPs for biomedical applications: PLGA and PLA, as well as a PLGA-PEG block copolymer (**Figure 6**). Here, the loading with R18/F5-TPB was reduced to 5 wt%, as this was shown previously to being optimal in terms of brightness for PLGA NPs.[21] The range of measured QYs for polyesters were between approximately 70% for the highest and roughly 30% for the lowest measured QYs, and thus in a range similar to those for methacrylate based polymers (*vide supra*). It should be noted, however, that the loading was significantly lower for polyesters, which is generally connected with higher QYs, indicating that at similar loading the QYs would be higher for methacrylate based polymers, as observed previously.[21] For PLGA and PLA, which bear terminal acid functions, NPs prepared in phosphate buffer were smaller than those prepared in MilliQ water. This is in agreement with previous results and was attributed to a more effective deprotonation of the acid groups in phosphate buffer, increasing the

effective charge fraction on the polymers.[12,19] In the case of PLGA-PEG, which does not bear acid groups and does not rely on charges for particle stabilization, no significant influence of the aqueous phase was detected.

In the case of PLGA a clear influence of mixing was observed for NPs prepared in MilliQ water, as observed previously,[20] where fast mixing using the impact-jet micromixer led to a strong decrease in the particle size from >100 nm to less than 50 nm, and to an increase in the QY from 30 to nearly 70%. Interestingly, this effect was much less expressed in phosphate buffer, both, for the size and for the QY. In the case of the PLGA-PEG block copolymer, NPs between 37 and 43 nm have been obtained, whatever the conditions of assembly, indicating that mixing had no significant influence on NP formation for this polymer. Nevertheless, PLGA-PEG based NPs made through fast mixing showed significantly higher QYs than those prepared manually. For PLA, finally, fast microfluidic mixing gave smaller NP sizes and higher QYs in both, MilliQ water and phosphate buffer, with the stronger effect being observed in water. Comparison of normalized absorbance spectra of PLGA, PLGA-PEG, and PLA based NPs prepared in MilliQ water, showed for PLGA and PLGA-PEG a small decrease in the absorbance at the shoulder (~530 nm, relative to the maximum) for preparation using fast microfluidic mixing (Supporting Information Figure S3 E), in good agreement with previous results on PLGA.[20]

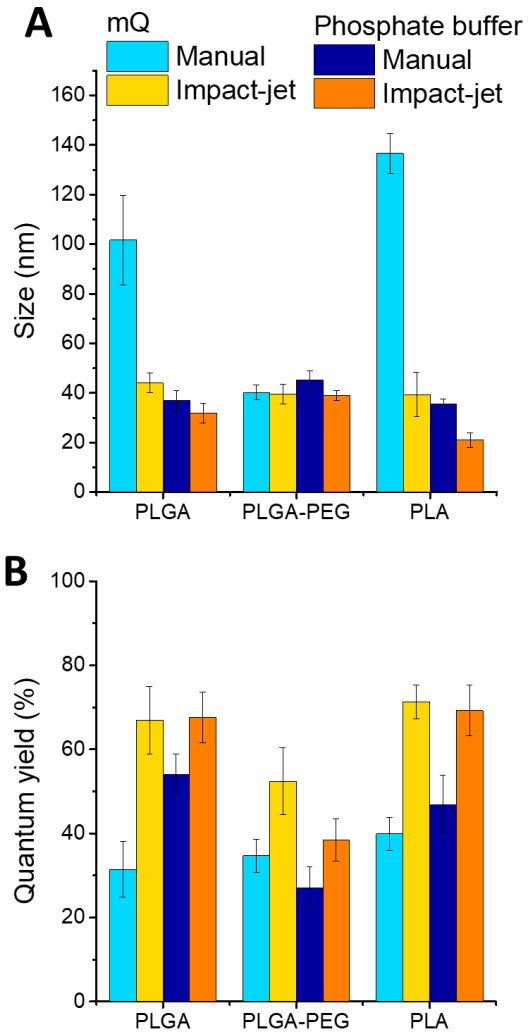

Figure 6. Size (A) and QY (B) of NPs of PLGA, PLGA-PEG and PLA, with 5 wt% dye (R18/F5TPB) prepared using the impact-jet mixer and manual nanoprecipitation in MilliQ water (mQ) or phosphate buffer. Mean values for three independent preparations are given. Error bars correspond to standard error of the mean. The flow rates for the impact-jet micromixer was set to 5 mL.min^{-1}.

Discussion

In order to differentiate the relative effects of nature of polymer (or polymer chemistry), and mixing on the formation of loaded polymer NPs, we tested several aspects of polymer chemistry (variation of backbone and different hydrophobic, hydrophilic, and charged side chains and their ratios) in two types of mixing: manual mixing, resulting in a mixing time of several tens of milliseconds, and microfluidics-based mixing using an impact-jet micromixer, which resulted in mixing times on the microsecond timescale. We can first distinguish the polymers considering whether the size of the formed NPs depended on mixing, or whether it is independent of the type and speed of mixing. The latter group includes the PEMA-COOH and PEMA-SO_3H polymers and PLGA (when precipitated in phosphate buffer), and PLGA-PEG. These were the polymers having the lowest solubility limits, typically below 15 vol% of water. Among the systems, where mixing matters, we find the EMA/HEMA copolymers, PLA,

but also PLGA when precipitated in MilliQ water. These had generally higher limits of solubility when mixing with the aqueous phase. Overall this indicates that the most "hydrophobic" polymers are insensitive (or less sensitive) to mixing, while mixing plays a decisive role in case of the less hydrophobic ones.

It should also be noted, that charged groups might play an important role in reducing the influence of mixing. Indeed, while nanoprecipitation of PLGA, which bears a terminal COOH group, was independent of mixing in phosphate buffer, in which charged groups have been shown to have a bigger influence[12], it became sensitive to mixing in MilliQ water (**Figure 6A**). Similarly, nanoprecipitation of PEMA-COOH polymers in MilliQ water also gave smaller NPs for faster mixing (**ESI Figure S5**, though in MilliQ water much larger NPs were formed in all cases). On the contrary, in the case of polymers relying on uncharged hydrophilic PEG or HEMA groups for the stabilization of forming particles, no dependence of the behavior on the used aqueous phase was detected: Nanoprecipitation of the block copolymer PLGA-b-PEG was insensitive to mixing speed in both phosphate buffer and MilliQ water (Figure 6A), while that of EMA/HEMA copolymers remained sensitive to mixing in both media (**Figure 5A** and **ESI Figure S6**). Interestingly, in case of PLGA-b-PEG the overall solubility seems to be controlled by the hydrophobic block, while the insensitivity to mixing hints to a particular type of stabilization achieved in the case of hydrophobic/hydrophilic block copolymers. We did not carry out a dedicated study of the particle stability over time for the different preparation approaches. However, in all cases, the NPs were stable over at least one week, the timescale, where experiments were typically carried out. The influences discussed below thus include stabilization over this time scale.

These observations can be rationalized based on previous considerations on the influence of mixing on nanoprecipitation: It is generally assumed that particle formation in nanoprecipitation becomes sensitive to mixing, when the characteristic mixing time (τ_{mix}) is larger than a critical or threshold time (τ_{crit} , typically system and condition dependent), while it is practically independent of mixing if $\tau_{mix} < \tau_{crit}$ (*i.e.* for fast mixing).[31,33,36,37]

At a molecular level, this has been interpreted in terms of the relative speeds of three processes: mixing of the aqueous and organic phases, associated with the mixing time (τ_{mix}), reorganization or collapse of the polymer chains (with characteristic time τ_{col}), and the encounter of polymer chains due to diffusion (τ_{dif}). [36,38,39] In case of fast mixing, chain collapse is thought to be faster than the diffusional encounter of polymer chains. In this case, deswelling and collapse of polymer chains lead to the formation of primary particles in a diffusion controlled process with little or no influence of the actual mixing on particle formation. On the other hand, if mixing is slow (large $\tau_{mix} > \tau_{crit}$), a gradual deswelling and collapse of the polymer chains is expected, leading to an increase of the effective collapse time of the chains, with $\tau_{col} \sim \tau_{mix}$. In consequence, diffusional encounters of chains compete with their

reorganization alongside particle formation, leading to a distinct influence of the speed of mixing on particle formation. (More precisely the critical mixing time was supposed to be $\tau_{crit} \geq 5\ \tau_{dif}$[36])

Here, we have shown that polymer chemistry influences the limiting water fraction leading to precipitation. In case of the most hydrophobic polymers, addition of only a tiny amount of water (~ 10%) was sufficient to reach the polymer solubility limit. We hypothesize that more hydrophobic polymers would therefore have a lower "effective" mixing time, corresponding to the time required for the water fraction to reach locally the solubility limit of the polymer. This lower "effective" mixing time would then lie below the critical time, independently of the global mixing speed. In this picture, the most hydrophobic polymers would collapse/reorganize at very low water fractions and therefore faster than the encounter of polymer chains due to diffusion, even at "slower" global mixing, leading to the observed decoupling of mixing and particle formation. In consequence, the speed of mixing (over the studied range of mixing times) does not have a significant influence for these polymers. Concerning charged groups, it has been found that particle growth is limited by the stabilization of the particles, notably through the build-up of sufficient surface charge or steric repulsion.[17,38,40,41] We assume that for polymers bearing more charged groups, stabilization is more effective, further reducing the influence of the speed of mixing.

In case of less hydrophobic polymers, e.g. the EMA/HEMA copolymers, a much higher water fraction (>20%), and therefore more complete mixing, is required to reach the solubility limit of the polymers. We suppose that in this case the global mixing time becomes the determining factor, and, as explained above, particle formation becomes sensitive to mixing at slower global mixing ($\tau_{mix} > \tau_{crit}$). In other words, in case of less hydrophobic polymers and slow mixing, the diffusion of sufficient water to lead to deswelling of the polymer could compete with diffusion of the polymers themselves, resulting in a process, where reorganization and particle formation occur at the same time. Such a scenario has been linked previously to the formation of larger particles with broader size distributions,[5,36,41] as observed here for the EMA/HEMA copolymers.

The influence (or absence of influence) of mixing on the encapsulation of the load was monitored here through absorbance and fluorescence measurements and notably the fluorescence QY. Decreasing QY can be linked to increasing aggregation of the dye molecules, leading notably to the formation of dye clusters within the polymer matrix, characterized by lower QY.[21,35,42] Here, in the case of the polyester systems prepared using slower manual mixing that showed lower QY, notably PLGA and PLGA-PEG, the relative absorbance at the shoulder (530 nm) was higher than for those prepared using fast microfluidic mixing. Such a spectroscopic signature has been linked to increasing dye aggregation.[43] Our previous results confirmed that this is also connected to smaller inter-dye distances and inhomogenities in the dye-loaded polymer NPs,[21] which all point into the direction of the formation of dye aggregates within the NPs, though their actual size could not be measured.

In practically all cases, the influence of mixing on the QY overlapped with the influences on particle size. This could be explained by the fact that in case of the most hydrophobic polymers "phase separation" of the polymer, leading to collapsed chains or primary particles occurs very rapidly. In the following, the dye salt could then adhere, in a diffusion limited process, to these primary polymer particles, and finally be integrated inside NPs upon aggregation of different polymer chains or primary particles. This would be expected to lead to a minimal aggregation of dye molecules within the particles. In case of less hydrophobic polymers, the solubility limit of the dye, which is of the order of 6 vol% of aqueous phase, can be reached significantly before the solubility limit of the polymer (>15%). In consequence, formation of dye aggregates is favored in the early stages of precipitation, these dye aggregates are then integrated into the NPs once the polymer reaches its solubility limit leading to its precipitation. Slow mixing would therefore lead to a longer time during which the dye salt starts to aggregate before the polymer starts doing so, resulting in more pronounced dye-aggregate formation, and lower QYs. Which is consistent with previously observed lower QYs and smaller distances between dyes in the case of NPs made from less hydrophobic polymers.[21] Fast mixing would again lead more quickly to a situation, where both, dye salt and polymer, are insoluble, leading to more homogeneous integration of the dyes, and therefore less dye aggregation and higher QYs

Conclusions

Nanoprecipitation is a key process for the assembly of loaded polymer NPs, in particular for biomedical applications. At the same time, it is a typical kinetically controlled process, where the process parameters have a strong influence on the obtained particles, and where the load can be kinetically trapped inside the NPs. On the other hand, the chemical nature of the compounds that are nanoprecipitated also has a significant influence on the obtained NPs, their size, loading and other properties. Within this study, we evaluated the relative influence of speed of mixing, a key processing parameter, and the chemical nature of the used polymers, i.e. the chemistry of the main and side chains. For this we compared two mixing approaches, "fast" microfluidic mixing using an impact-jet micromixer (micromixing time in the range of <1 to 3 ms), and "slow" manual mixing (several tens of ms scale), while varying hydrophobicity, backbone, presence of charged groups, and architecture of the used polymers. Our results showed that the influence of the mixing process depends on the nature of the polymer. In particular, formation of NPs from polymers with high hydrophobicity bearing charged groups became practically independent of the speed of mixing, in terms of size and loading. In this case, variations of particle size from about 20 nm to nearly 200 nm and of QYs from 30 to 75% were observed depending nearly exclusively on the polymer chemistry, with practically no influence of the mixing speed. On the other hand, a clear influence of the speed of mixing was observed in the case of less hydrophobic polymers, in particular the important polyesters PLGA and PLGA, leading to

the formation of up to three times bigger NPs with larger size distribution and up to two times lower fluorescence QYs at slower mixing. Whether the mixing speed played a role, or not, was directly correlated with the solubility limit of the polymers in acetonitrile-water mixtures as obtained from simple turbidimetry measurements, with a critical point for solubility limits between 15 and 20 vol% water. Quite simple evaluation of the polymer, experimentally or theoretically, can therefore be used to predict its behavior during particle assembly on a quantitative basis. A quite interesting result is also the fact that some systems show only a very small influence of mixing, as this could facilitate scale-up. On the one hand, this could help fine tuning the size, loading and release of loaded polymer NPs and through this their biomedical properties. On the other hand, such knowledge should facilitate designing the production of loaded polymer NPs, which is a question with increasing importance as various types of NPs make their way to large scale biomedical applications.

Supporting Information

Details of polymer synthesis, detailed geometry and further results for CFD simulation, absorbance and emission spectra of dye-loaded nanoparticles, additional DLS, ζ-potential, and quantum yield measurements.

Acknowledgements

This work was supported by an FRC Emerging Investigators grant, and by the "Prix Espoirs de l'Université de Strasbourg". The authors acknowledge the support and the use of resources of the French Infrastructure for Integrated Structural Biology FRISBI ANR-10-INBS-05 and of Instruct-ERIC and especially C. Crucifix for help with electron microscopy.

References

(1) Banik, B. L.; Fattahi, P.; Brown, J. L. Polymeric Nanoparticles: The Future of Nanomedicine. *Wiley Interdiscip. Rev. Nanomed. Nanobiotechnol.* **2016**, *8* (2), 271–299. https://doi.org/10.1002/wnan.1364.

(2) Shi, J.; Kantoff, P. W.; Wooster, R.; Farokhzad, O. C. Cancer Nanomedicine: Progress, Challenges and Opportunities. *Nat. Rev. Cancer* **2017**, *17* (1), 20–37. https://doi.org/10.1038/nrc.2016.108.

(3) D'Addio, S. M.; Prud'homme, R. K. Controlling Drug Nanoparticle Formation by Rapid Precipitation. *Adv. Drug Deliv. Rev.* **2011**, *63* (6), 417–426. https://doi.org/10.1016/j.addr.2011.04.005.

(4) Martínez Rivas, C. J.; Tarhini, M.; Badri, W.; Miladi, K.; Greige-Gerges, H.; Nazari, Q. A.; Galindo Rodríguez, S. A.; Román, R. Á.; Fessi, H.; Elaissari, A. Nanoprecipitation Process: From Encapsulation to Drug Delivery. *Int. J. Pharm.* **2017**, *532* (1), 66–81. https://doi.org/10.1016/j.ijpharm.2017.08.064.

(5) Liu, Y.; Yang, G.; Zou, D.; Hui, Y.; Nigam, K.; Middelberg, A. P. J.; Zhao, C.-X. Formulation of Nanoparticles Using Mixing-Induced Nanoprecipitation for Drug Delivery. *Ind. Eng. Chem. Res.* **2020**, *59* (9), 4134–4149. https://doi.org/10.1021/acs.iecr.9b04747.

(6) Yan, X.; Bernard, J.; Ganachaud, F. Nanoprecipitation as a Simple and Straightforward Process to Create Complex Polymeric Colloidal Morphologies. *Adv. Colloid Interface Sci.* **2021**, *294*, 102474. https://doi.org/10.1016/j.cis.2021.102474.

(7) Fessi, H.; Puisieux, F.; Devissaguet, J. Ph.; Ammoury, N.; Benita, S. Nanocapsule Formation by Interfacial Polymer Deposition Following Solvent Displacement. *Int. J. Pharm.* **1989**, *55* (1), R1–R4. https://doi.org/10.1016/0378-5173(89)90281-0.

(8) Karnik, R.; Gu, F.; Basto, P.; Cannizzaro, C.; Dean, L.; Kyei-Manu, W.; Langer, R.; Farokhzad, O. C. Microfluidic Platform for Controlled Synthesis of Polymeric Nanoparticles. *Nano Lett.* **2008**, *8* (9), 2906–2912. https://doi.org/10.1021/nl801736q.

(9) Markwalter, C. E.; Prud'homme, R. K. Design of a Small-Scale Multi-Inlet Vortex Mixer for Scalable Nanoparticle Production and Application to the Encapsulation of Biologics by Inverse Flash NanoPrecipitation. *J. Pharm. Sci.* **2018**, *107* (9), 2465–2471. https://doi.org/10.1016/j.xphs.2018.05.003.

(10) Ding, S.; Anton, N.; Vandamme, T. F.; Serra, C. A. Microfluidic Nanoprecipitation Systems for Preparing Pure Drug or Polymeric Drug Loaded Nanoparticles: An Overview. *Expert Opin. Drug Deliv.* **2016**, *13* (10), 1447–1460. https://doi.org/10.1080/17425247.2016.1193151.

(11) Lince, F.; Marchisio, D. L.; Barresi, A. A. Strategies to Control the Particle Size Distribution of Poly-ε-Caprolactone Nanoparticles for Pharmaceutical Applications. *J. Colloid Interface Sci.* **2008**, *322* (2), 505–515. https://doi.org/10.1016/j.jcis.2008.03.033.

(12) Reisch, A.; Runser, A.; Arntz, Y.; Mély, Y.; Klymchenko, A. S. Charge-Controlled Nanoprecipitation as a Modular Approach to Ultrasmall Polymer Nanocarriers: Making Bright and Stable Nanoparticles. *ACS Nano* **2015**, *9*, 5104–5116. https://doi.org/10.1021/acsnano.5b00214.

(13) Bovone, G.; Cousin, L.; Steiner, F.; Tibbitt, M. W. Solvent Controls Nanoparticle Size during Nanoprecipitation by Limiting Block Copolymer Assembly. *Macromolecules* **2022**, *55* (18), 8040–8048. https://doi.org/10.1021/acs.macromol.2c00907.

(14) Lavino, A. D.; Ferrari, M.; Barresi, A. A.; Marchisio, D. Effect of Different Good Solvents in Flash Nano-Precipitation via Multi-Scale Population Balance Modeling-CFD Coupling Approach. *Chem. Eng. Sci.* **2021**, *245*, 116833. https://doi.org/10.1016/j.ces.2021.116833.

(15) Pagels, R. F.; Edelstein, J.; Tang, C.; Prud'homme, R. K. Controlling and Predicting Nanoparticle Formation by Block Copolymer Directed Rapid Precipitations. *Nano Lett.* **2018**, *18* (2), 1139–1144. https://doi.org/10.1021/acs.nanolett.7b04674.

(16) Roger, K.; Eissa, M.; Elaissari, A.; Cabane, B. Surface Charge of Polymer Particles in Water: The Role of Ionic End-Groups. *Langmuir* **2013**, *29* (36), 11244–11250. https://doi.org/10.1021/la4019053.

(17) Zhang, C.; Pansare, V. J.; Prud'homme, R. K.; Priestley, R. D. Flash Nanoprecipitation of Polystyrene Nanoparticles. *Soft Matter* **2011**, *8* (1), 86–93. https://doi.org/10.1039/C1SM06182H.

(18) Egloff, S.; Runser, A.; Klymchenko, A.; Reisch, A. Size-Dependent Electroporation of Dye-Loaded Polymer Nanoparticles for Efficient and Safe Intracellular Delivery. *Small Methods* **2021**, *5* (2), 2000947. https://doi.org/10.1002/smtd.202000947.

(19) Rosiuk, V.; Runser, A.; Klymchenko, A.; Reisch, A. Controlling Size and Fluorescence of Dye-Loaded Polymer Nanoparticles through Polymer Design. *Langmuir* **2019**, *35* (21), 7009–7017. https://doi.org/10.1021/acs.langmuir.9b00721.

(20) Chen, H.; Celik, A. E.; Mutschler, A.; Combes, A.; Runser, A.; Klymchenko, A. S.; Lecommandoux, S.; Serra, C. A.; Reisch, A. Assembly of Fluorescent Polymer Nanoparticles Using Different Microfluidic Mixers. *Langmuir* **2022**. https://doi.org/10.1021/acs.langmuir.2c00534.

(21) Reisch, A.; Trofymchuk, K.; Runser, A.; Fleith, G.; Rawiso, M.; Klymchenko, A. S. Tailoring Fluorescence Brightness and Switching of Nanoparticles through Dye Organization in the Polymer Matrix. *ACS Appl. Mater. Interfaces* **2017**, *9* (49), 43030–43042. https://doi.org/10.1021/acsami.7b12292.

(22) Reisch, A.; Didier, P.; Richert, L.; Oncul, S.; Arntz, Y.; Mély, Y.; Klymchenko, A. S. Collective Fluorescence Switching of Counterion-Assembled Dyes in Polymer Nanoparticles. *Nat. Commun.* **2014**, *5*, 4089. https://doi.org/10.1038/ncomms5089.

(23) Nagasawa, H.; Aoki, N.; Mae, K. Design of a New Micromixer for Instant Mixing Based on the Collision of Micro Segments. *Chem. Eng. Technol.* **2005**, *28* (3), 324–330. https://doi.org/10.1002/ceat.200407118.
(24) Cunningham, G. P.; Vidulich, G. A.; Kay, R. L. Several Properties of Acetonitrile-Water, Acetonitrile-Methanol, and Ethylene Carbonate-Water Systems. *J. Chem. Eng. Data* **1967**, *12* (3), 336–337. https://doi.org/10.1021/je60034a013.
(25) Galvão, A. C.; Robazza, W. S.; Rodrigues, D. Refratometric Study of Ternary Mixtures Formed by Water, Glucose and Acetonitrile at Temperatures Ranging from 293 K to 333 K. *Phys. Chem. Liq.* **2016**, *54* (1), 56–61. https://doi.org/10.1080/00319104.2015.1068664.
(26) Würth, C.; Grabolle, M.; Pauli, J.; Spieles, M.; Resch-Genger, U. Comparison of Methods and Achievable Uncertainties for the Relative and Absolute Measurement of Photoluminescence Quantum Yields. *Anal. Chem.* **2011**, *83* (9), 3431–3439. https://doi.org/10.1021/ac2000303.
(27) Commenge, J.-M.; Falk, L. Villermaux–Dushman Protocol for Experimental Characterization of Micromixers. *Chem. Eng. Process. Process Intensif.* **2011**, *50* (10), 979–990. https://doi.org/10.1016/j.cep.2011.06.006.
(28) Winkelmann, J. Diffusion Coefficient of Acetonitrile in Water. In *Diffusion in Gases, Liquids and Electrolytes*; Lechner, M. D., Ed.; Springer Berlin Heidelberg: Berlin, Heidelberg, 2018; pp 236–239. https://doi.org/10.1007/978-3-662-54089-3_141.
(29) Lince, F.; Marchisio, D. L.; Barresi, A. A. A Comparative Study for Nanoparticle Production with Passive Mixers via Solvent-Displacement: Use of CFD Models for Optimization and Design. *Chem. Eng. Process. Process Intensif.* **2011**, *50* (4), 356–368. https://doi.org/10.1016/j.cep.2011.02.015.
(30) Bourne, J. R. Mixing and the Selectivity of Chemical Reactions. *Org. Process Res. Dev.* **2003**, *7* (4), 471–508. https://doi.org/10.1021/op020074q.
(31) Johnson, B. K.; Prud'homme, R. K. Chemical Processing and Micromixing in Confined Impinging Jets. *AIChE J.* **2003**, *49* (9), 2264–2282. https://doi.org/10.1002/aic.690490905.
(32) Falk, L.; Commenge, J.-M. Performance Comparison of Micromixers. *Chem. Eng. Sci.* **2010**, *65* (1), 405–411. https://doi.org/10.1016/j.ces.2009.05.045.
(33) Liu, Y.; Cheng, C.; Liu, Y.; Prud'homme, R. K.; Fox, R. O. Mixing in a Multi-Inlet Vortex Mixer (MIVM) for Flash Nano-Precipitation. *Chem. Eng. Sci.* **2008**, *63* (11), 2829–2842. https://doi.org/10.1016/j.ces.2007.10.020.
(34) Reisch, A.; Heimburger, D.; Ernst, P.; Runser, A.; Didier, P.; Dujardin, D.; Klymchenko, A. S. Protein-Sized Dye-Loaded Polymer Nanoparticles for Free Particle Diffusion in Cytosol. *Adv. Funct. Mater.* **2018**, *28* (48), 1805157. https://doi.org/10.1002/adfm.201805157.
(35) Andreiuk, B.; Reisch, A.; Bernhardt, E.; Klymchenko, A. S. Fighting Aggregation-Caused Quenching and Leakage of Dyes in Fluorescent Polymer Nanoparticles: Universal Role of Counterion. *Chem. – Asian J.* **2019**, *14* (6), 836–846. https://doi.org/10.1002/asia.201801592.
(36) Nikoubashman, A.; Lee, V. E.; Sosa, C.; Prud'homme, R. K.; Priestley, R. D.; Panagiotopoulos, A. Z. Directed Assembly of Soft Colloids through Rapid Solvent Exchange. *ACS Nano* **2016**, *10* (1), 1425–1433. https://doi.org/10.1021/acsnano.5b06890.
(37) Li, N.; Nikoubashman, A.; Panagiotopoulos, A. Z. Multi-Scale Simulations of Polymeric Nanoparticle Aggregation during Rapid Solvent Exchange. *J. Chem. Phys.* **2018**, *149* (8), 084904. https://doi.org/10.1063/1.5046159.
(38) Cheng, J. C.; Vigil, R. D.; Fox, R. O. A Competitive Aggregation Model for Flash NanoPrecipitation. *J. Colloid Interface Sci.* **2010**, *351* (2), 330–342. https://doi.org/10.1016/j.jcis.2010.07.066.
(39) Lavino, A. D.; Di Pasquale, N.; Carbone, P.; Marchisio, D. L. A Novel Multiscale Model for the Simulation of Polymer Flash Nano-Precipitation. *Chem. Eng. Sci.* **2017**, *171*, 485–494. https://doi.org/10.1016/j.ces.2017.04.047.
(40) Morozova, T. I.; Lee, V. E.; Panagiotopoulos, A. Z.; Prud'homme, R. K.; Priestley, R. D.; Nikoubashman, A. On the Stability of Polymeric Nanoparticles Fabricated through Rapid Solvent Mixing. *Langmuir* **2019**, *35* (3), 709–717. https://doi.org/10.1021/acs.langmuir.8b03399.

(41) Botet, R.; Roger, K. How Do Interactions Control Droplet Size during Nanoprecipitation? *Curr. Opin. Colloid Interface Sci.* **2016**, *22*, 108–112. https://doi.org/10.1016/j.cocis.2016.03.003.
(42) Ashoka, A. H.; Aparin, I. O.; Reisch, A.; Klymchenko, A. S. Brightness of Fluorescent Organic Nanomaterials. *Chem. Soc. Rev.* **2023**. https://doi.org/10.1039/D2CS00464J.
(43) Macdonald, R. I. Characteristics of Self-Quenching of the Fluorescence of Lipid-Conjugated Rhodamine in Membranes. *J. Biol. Chem.* **1990**, *265*, 13533–13539.